Monitoring pattern formation in drying and wetting dispersions of gold nanoparticles by ESEM†

Casper Kunstmann-Olsen[a], Domagoj Belić[a] and Mathias Brust[a]*

Received Xth XXXXXXXXXX 20XX, Accepted Xth XXXXXXXXX 20XX
First published on the web Xth XXXXXXXXXX 200X
DOI: 10.1039/c000000x

We report an investigation of the self-assembly of patterns from functionalized gold nanoparticles (GNPs) by monitoring the process *in-situ* by environmental scanning electron microscopy (ESEM) during both evaporation and condensation of the dispersant. As this method limits the choice of dispersants to water, GNPs functionalized with hydrophilic thiol-ligands, containing poly(ethylene)glycol (PEG) groups, were used on a variety of substrates including pre-patterned ones. Particular emphasis was given to early stage deposition of GNPs, as well as re-dispersion and lift off upon condensation of water droplets. ESEM presents a unique opportunity of directly imaging such events *in-situ*. It was found that attractive interactions between the substrate and the GNPs are often stronger than expected once the particles have been deposited. The role of nickel perchlorate as a highly water-soluble additive has been studied. It was found that entropically driven deposition of particles and decoration of surface features was enhanced in its presence, as expected.

1 Introduction

The formation of complex patterns as well as regular superlattices in two and three dimensions from drying dispersions of nanoparticles has been a key topic in scientific research since the burgeoning of chemical nanoscale science in the early 1990s.[1,2] Such phenomena are not only of considerable fundamental interest, but also suggest possibilities of creating new 2- and 3-dimensional materials through the controlled assembly of the constituent nanoparticles.[3] Materials and thin films of this type could find applications as optical or conductive coatings, in information storage and as sensors, to name only a few possibilities. Since the formation of drying patterns from dispersions of particulate matter as well as the flocculation of destabilized colloids are phenomena that have been known and studied for a very long time, it is somewhat arbitrary to point to a single study that could be regarded as the first among the more recent publica-

† Electronic Supplementary Information (ESI) available: TEM images, additional SEM images and videos are available. See DOI: 10.1039/c000000x/

[a] *Dept. of Chemistry, University of Liverpool, Crown Street, L69 7LD Liverpool, United Kingdom. E-mail: mbrust@liv.ac.uk*

tions on nanoscale pattern formation from dispersed nanoparticles. Nevertheless, for the purpose and scope of this discussion article, it is appropriate to begin with Giersig and Mulvaney's work on the formation of two-dimensional superlattices by electrophoretic deposition of monodisperse gold nanoparticles with and without thiolate ligands on amorphous carbon substrates.[4,5] To our knowledge, that work demonstrated for the first time a phenomenon that nowadays is seen practically on a daily basis in many electron microscopic studies of all kinds of nanoparticles deposited on a suitable substrate. The perhaps most widely recognized example of pattern formation from colloidal particles was the finding by Bawendi and coworkers, that ligand capped CdSe nanocrystals spontaneously formed highly ordered superlattices in two- and, to some extent, three dimensions, upon evaporation of the solvent.[6] This coincided with Pileni and coworkers' discovery of such new materials formed from Ag_2S nanoparticles[7] and was followed by Whetten et al. reporting superlattice formation from thiolate-capped gold nanoparticles upon evaporation of their dispersions in toluene.[8] Countless further examples followed over the years, most notably the impressive body of work by Murray and coworkers, that includes a huge range of materials of different sizes and shapes, as well as combinations of different nanomaterials.[9]

Surprisingly, the conditions that have to be fulfilled in order to obtain highly ordered superlattices are still not well understood. The ability to prepare samples of extraordinarily high monodisperity has originally been suggested as one important factor; indeed, the formation of the superlattice was argued to be a marker for monodispersity,[6] whereas Landman *et al.* argued, based on molecular mechanics simulations of thiolate-capped gold clusters, that the interaction between interdigitated bundles of ligands played an important role.[10] Since then, superlattices with bimodal size distributions,[11,12] spontaneous size segregation, and those of Au nanoparticles (and many others) without thiolate ligands[13] have been reported, indicating that neither monodispersity nor a particular constitution of the ligand shell are necessary conditions for this phenomenon to occur. Klabunde and coworkers have shown that in the presence of excess thiol, thiolate-capped gold nanoparticles formed near perfect superlattices over large areas, while in the absence of excess thiol, much less perfect lattices of limited extension were obtained.[14] In general, the presence of soluble contaminants appears to favour the formation of superlattices and supracrystals, which has therefore been tentatively attributed to entropy driven colloidal crystallization.[15]

On the other hand, the majority of nanoparticle preparation methods lead to more complicated and less ordered drying patterns. Examples include coffee cup drying circles,[16] foam-like cellular networks and worm-like aggregates of nanoparticles. These structures have been attributed to long-range self-organization phenomena far from equilibrium driven by external forces such as dewetting. Different models have been applied to account for the various types of patterns observed, including spinodal phase separation,[17,18] hydrodynamic effects (Benard-Marangoni convection)[19], and nucleation phenomena.[20]

Given the wealth of different structures formed, and crystalline order being an exception rather than the rule, it is evident that a number of different parameters

contribute to determining the outcome of each drying experiment and that the behaviour of a drying dispersion of nanoparticles is complex. Most reports have used either TEM or AFM to image the patterns formed, with AFM perhaps being the more versatile of the two techniques, because any type of flat substrate can be used and surfaces that are still covered by liquid can be imaged.[21] On the other hand, it is a relatively slow technique, prone to imaging artefacts, so the imaging process itself can significantly affect the imaged pattern. Alivisatos and coworkers have used liquid cell TEM to monitor *in-situ* superlattice formation of Pt particles.[22] Similarly, here we evaluate the use of environmental scanning electron microscopy (ESEM) as a tool to interrogate *in-situ* both drying and wetting processes of aqueous dispersions of gold nanoparticles on a range of different substrates, including pre-patterned ones. The spontaneous decoration of surface features, such as grooves, by nanoparticles is a well studied phenomenon.[23–27] We have encountered a plethora of different patterns which are often coexistent on one single sample indicating the presence of strong local effects, for example step edges on HOPG, that interfere with the flow and drying of the dispersant. While we have obtained a large number of sometimes strikingly appealing images, the study is still preliminary and should give plenty of scope for fruitful discussions. In particular, we wish to emphasize the role of particle-particle and particle-substrate interaction, which in most of the cases studied here appear to be stronger than expected.

2 Experimental

2.1 Particle preparation

Batches of gold nanoparticles typically in the 10-14 nm range, were prepared following the classic Turkevich citrate reduction method.[28] Briefly, 86 mg of *hydrogentetrachloroaurate trihydrate* ($HAuCL_4 \times 3H_2O$, Sigma Aldrich) was dissolved in 140 ml of DI water and brought to boil in a round bottom flask equipped with a reflux condenser. Then 20 ml of a near boiling hot aqueous solution of trisodium citrate (0.9 mM) was added rapidly through the condenser under vigorous stirring, and the mixture was refluxed for 30 min. After cooling the mixture down to room temperature, 13.6 mg (17 μMol) of *mercaptopolyethylenglycol* (PEG) polymer (MW: 800 g/mol) was added and dissolved by vigorous shaking of the flask. The mixture was allowed to react overnight and excess polymer was removed by repeated centrifugation and re-dispersion of the particles in water. These dispersions were used in all experiments, unless stated otherwise. The monodispersity of the preparations depends crucially on achieving ideal mixing conditions. For this reason experiments are reported using GNP samples of various "quality" in terms of their monodispersity.

2.2 Substrate preparations

Investigations carried out on Si surfaces were done on 4×4 mm wafers cut from a n-doped silicon $[100]$ wafer. Before usage the samples were cleaned with acetone and ethanol in a sonicator for 15 min in each solution and dried using Argon. These Si surfaces are normally covered with native oxide (around 1 nm)[29] and

are hydrophilic (contact angle $< 20°$).[30]
As a hydrophobic (contact angle $95 - 100°$)[31] and electrically conductive surface, freshly cleaved highly-ordered pyrolytic graphite (HOPG) was used (HOPG 3.5 ± 1.5 Mosaic, Agar Scientific).
Polydimethylsiloxane (PDMS, *Sylgard 184*, Sigma Aldrich) surfaces were prepared as per supplier instructions. 10 parts monomer was mixed with 1 part curing agent and evacuated under vacuum for 60 min to remove air bubbles. The mixture was then poured onto an objective glass slide (to form a 5 mm thin sheet) and cured for 60 min at $100°$C. The resulting surface is very flat and has a high contact angle with water($110°$).[32]
To create wrinkled PDMS, the method reported by Hiltl *et al.* was followed.[33] A 5 mm thin PDMS sheet (prepared as above) is stretched by 150% in one direction and exposed to an ambient air plasma for 120 s (200 mTorr at 30 W). As a result of the reaction of PDMS and oxygen from the plasma, the surface contains a thin film of silicon oxide. Hence, in terms of surface properties, this substrate is expected to behave similarly to the Si samples.

2.3 EM imaging

The main method of investigation in this work is ESEM using a FEI *Quanta 250* FEG SEM. This microscope has a sample chamber which utilizes differential pumping, allowing for samples to be held at pressures of up to 2700 Pa. The chamber is equipped with a Peltier cooling stage and can be filled with pure water vapour. By adjusting temperature and pressure, according to the water phase diagram of water, complete humidity control is possible, so that fully hydrated samples could be imaged. The ability to control both temperature and humidity of the sample is a major advantage, because it is known that these factors affect the GNP pattern formation.[34] Unless otherwise noted, all images presented here were obtained in ESEM mode under fairly high relative humidity ($> 50\%$).

While an electron beam can be used in many interesting ways to pattern surfaces,[35,36] SEM imaging is also known to to have a range of effects on the examined surface. For instance, it can affect the surface wettability, particle properties, induce surface heating, and even create free radicals.[37–41] Therefore, great care was taken to keep the beam energy and electron dose as low as possible (while still maintaining good image quality), in line with the methodology of Rykazcewski and coworkers.[42,43] Furthermore, frequent periods of beam-blanking were enforced to allow for dissipation of built up surface charge.

Transmission electron microscopy (TEM) measurements were carried out on a FEI *Tecnai G2 Spirit BioTWIN* TEM operating at 120 kV. Here, the samples were prepared by drop-casting the GNP solution onto amorphous carbon TEM grids. TEM images were analyzed using *ImageJ* software.

2.4 Drying and wetting experiments

To investigate pattern formation of GNP from solution, the substrate is mounted in the ESEM holder which is pre-cooled to $2°$C. A 1 μL droplet is deposited manually on its surface using a precision pipette. The chamber is then immediately

closed and pumped down to 900 Pa. This value is far above the dew-point of water (100% humidity corresponds to 709 Pa at this temperature). The microscope optics are then aligned and optimized and the chamber pressure slowly reduced in intervals of 20 Pa with resting periods of 5 min for every 100 Pa, causing gradual evaporation of the water.

For wetting experiments the sample was slowly dehydrated in the SEM chamber to around 50% humidity (400 Pa at 2°C) and the water vapour pressure was then slowly increased to the dew-point and beyond, while surface features were continuously imaged. As some substrates conduct heat better than others, the pressure is raised to at least 1300 Pa to ensure complete surface hydration.

2.5 Salting out experiments and Zeta-potential measurements

To create a 10 mM stock solution, 39.2 mg of *nickel(II) perchlorate* ($Ni(ClO_4)_2$) (Sigma Aldrich) was dissolved in 40 mL of DI water. By slowly evaporating the solution in the ESEM, it is possible to monitor the effect of a wide range of surface salt concentrations on GNP pattern formation. Similar studies using fixed salt concentrations showed a huge effect of salts on GNP self-assembly.[44,45]
Zeta-potentials of GNPs were measured as a function of nickel-perchlorate concentration, using a Zetasizer Nano Z (Malvern Instruments Ltd.). Average conductivity is also measured to ensure that the increasing electrolyte concentration does not influence the results.

3 Results and discussion

3.1 Drying patterns

All surface patterns were obtained by droplet deposition and hence consist of two parts: a boundary and an inner region. Usually, different self-organized nanostructures form in these regions. The boundary is characterized in all cases by a typical ring stain, which is attributable to droplet pinning.[46–48] When a water droplet is deposited on a surface, the wetting properties are determined by its hydrophobicity, which is measured by the contact angle. This again is a function of the surface composition and its geometry. The substrates used in this study have different wetting properties, ranging from hydrophilic Si to strongly hydrophobic PDMS and HOPG, whereas the GNP used were hydrophilic due to their PEG coating.
As explained above, the samples enter the ESEM fully hydrated at 100% relative humidity. As the vapour pressure in the ESEM decreases, the droplet shrinks as water evaporates. The ring pattern formation, caused by droplet pinning, was generally the first particle deposition phenomenon observed. This fixes the contact line of the droplet and prevents its further lateral shrinkage as more water evaporates.[46] This is observed on all types of substrates and is attributed to a strong inter-particle interaction, which forms highly packed sheets (see figure 1 for Si (*a*) and HOPG substrates (*b*)). The relative intensity of the particle layers (brighter areas) are directly proportional to the GNP layer thickness, analogous to the samples studied by Li *et al.* using HAADF-STEM.[49]

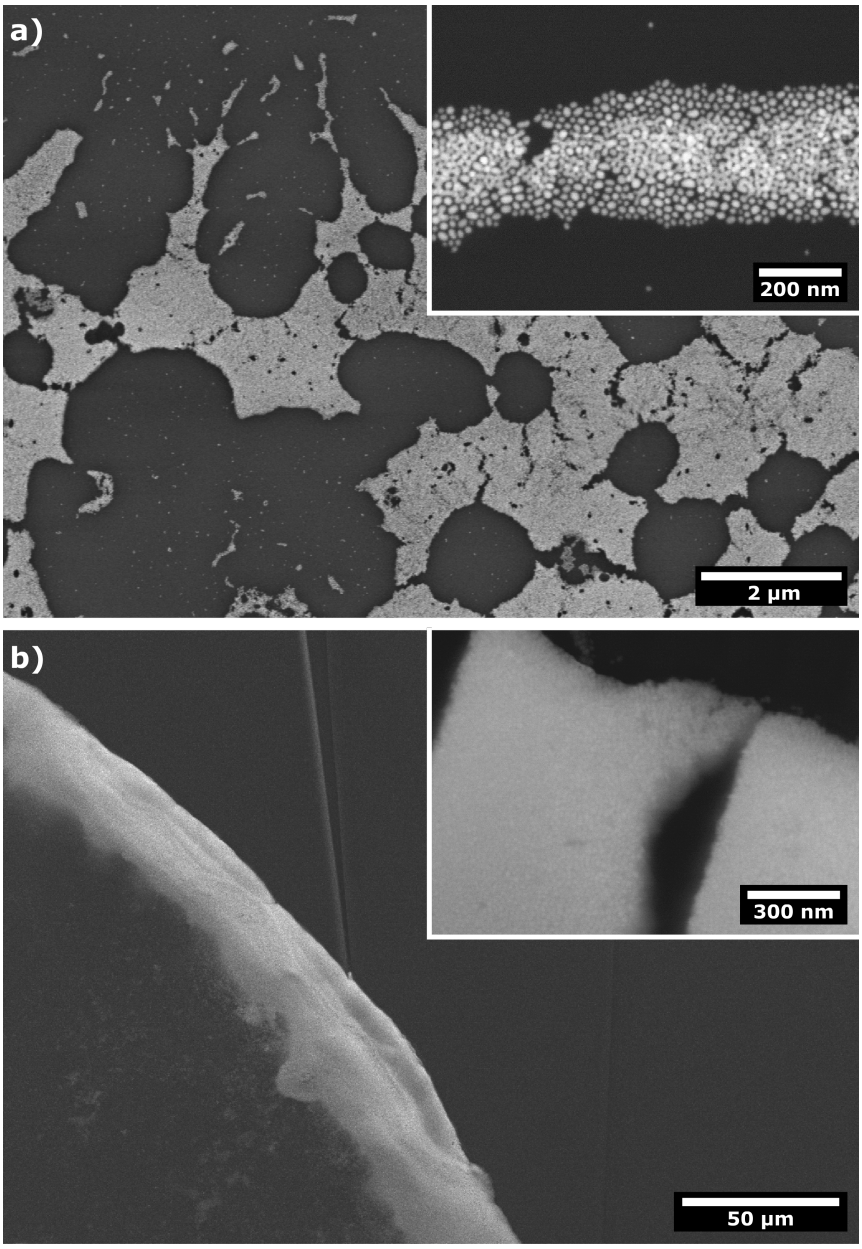

Fig. 1 SEM images showing almost solid sheets of closely packed GNPs on a Si surface (a) and the tightly packed ring stain on the outer boundary on a HOPG surface (b). Insets show close ups of the structures so that individual GNPs are visible.

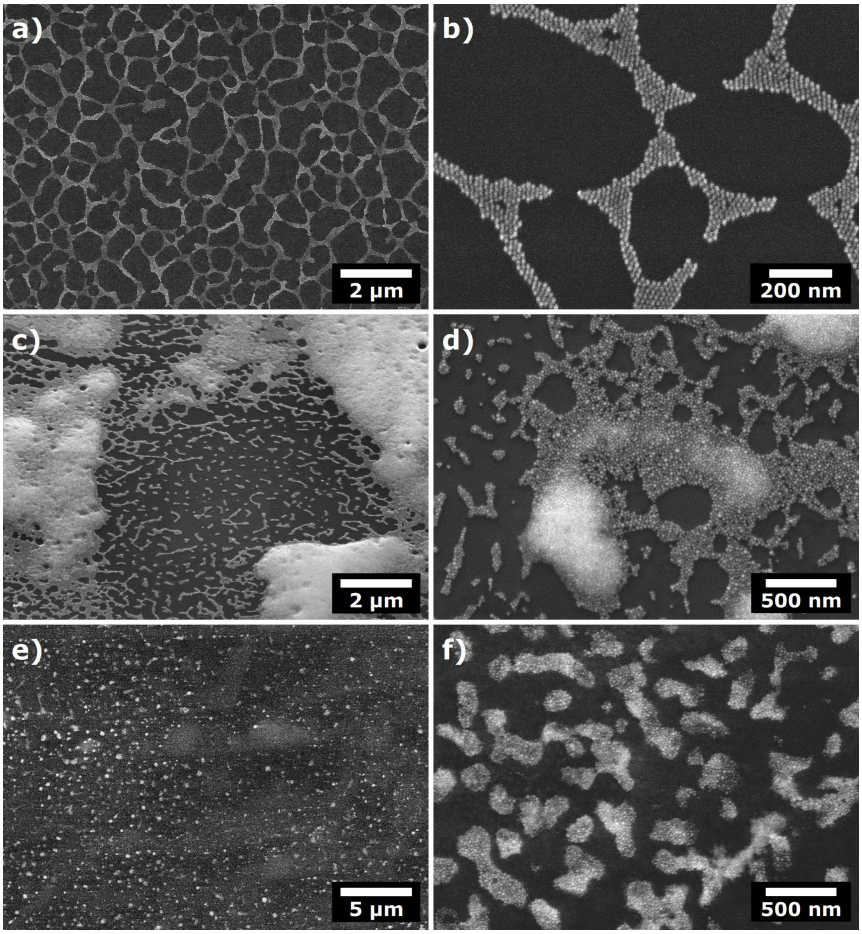

Fig. 2 Typical GNP pattern formation after drying, on Si (*a*+*b*), HOPG (*c*+*d*) and flat PDMS (*e*+*f*).

While the structure of the outer boundary were fairly consistent throughout all samples and surfaces, the inner structure was quite different (see figure 2).
Figure 2*a* and 2*b* show GNP deposited on a clean hydrophilic Si surface. As the water continues to evaporate, a thin-film of water was formed from which the GNP precipitate evenly over the surface. The resulting structure was two-dimensional consisting of less than a monolayer of particles. The pattern formed is consistent with spinodal phase separation first suggested by Ge and Brus for patterns formed from CdSe suspensions on HOPG.[18] This deposition occurs from dispersion when the evaporating dispersant is no longer able to screen attractive inter-particle forces. The role of the substrate is not usually considered within this model, which is clearly an oversimplification, as exemplified in the case of HOPG as a substrate (see figure 2*c*+*d*).
We attribute this behaviour to strong differences in solvent-substrate interactions. Due to the hydrophobicity of HOPG, the water film breaks up into droplets prior to or near the spinodal phase separation process. This results in the formation

of large 3D aggregates of particles reflecting the formation of individual dispersion droplets. Between these droplets the wormlike aggregates typical for the spinodal process are observed. In addition, the affinity between substrate and particles may be important. The hydrophilic particles are expected to interact stronger with the Si surface than with the HOPG. This is consistent with the observation of particle multilayers on the HOPG substrate, i.e. the PEG coated particles interact stronger with each other than with the surface.
This effect is expressed even more noticeably on PDMS (see figure 2*e*+*f*), which is even more hydrophobic than HOPG. Here the clustering effect is more pronounced as the water thin film quickly splits into smaller droplets during evaporation, thus enabling localized precipitation. Interestingly, spinodal effects are not observed on PDMS substrate.
Hexagonally packed superlattices of GNPs were also observed as a minority species on many samples. For example, figure 2*b* shows relatively small areas of such structures formed by highly monodisperse GNPs on Si. The same particles deposited on amorphous carbon TEM grids readily form the typical larger area superlattices (see ESI1). In most of our experiments the GNP solutions used were rather more polydisperse and did not show strong tendencies to form long-range hexagonally packed arrays. Based on our observations, except for the local packing effects, the polydispersity does not appear to influence the type of long-range patterns formed. Notably, size segregation and/or formation of superlattices with multimodal size distributions reported previously for polydispersed particles[11] have not been observed.

3.2 Wetting on HOPG

To investigate the wetting and redispersion properties of the different deposits, the ESEM procedure was reversed compared to that described in the previous section, i.e. the pressure, and hence the relative humidity, was slowly increased until condensation of water droplets on the sample surface was observed. Figure 3 shows how water droplets nucleate around GNP clusters and gradually grow on the HOPG surface.
As more and more water condenses around the particle clusters the water droplets grow and slowly coalesce, eventually forming microscopic (t = 261 s) droplets. In the final image (t = 919 s), the sample has been dried again, leaving a newly formed ring stain on the surface. Figure 4 shows a close up of this ring stain. Surprisingly, much of the initially deposited monolayer remains in place during the entire condensation and evaporation cycle. We attribute this to unexpectedly strong hydrophobic interactions between the substrate and the particles, which can be mediated through the polymeric ligand shell. A comparable behaviour of PEGylated GNPs, which adapted their affinity to solvents of different polarity, has previously been reported by Eychmüller and coworkers.[50]
Nevertheless, a significant amount of particles redispersed in the water droplets and redeposited upon renewed drying. This is seen more clearly at higher magnification in the inset in figure 4 (and figure ESI2†).
A further portion of the particles were lifted off the surface and later deposited in coherent sheets, held together by strong inter-particle interactions (see figure ESI2†). This effect turned out to be a recurrent theme in our experiments and

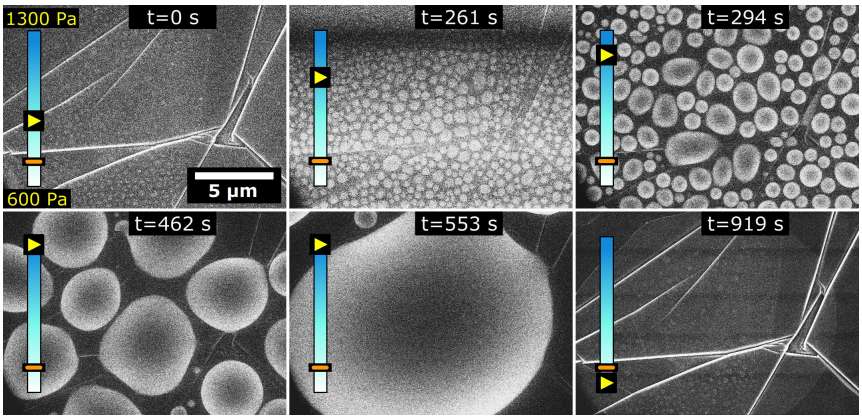

Fig. 3 Wetting of GNP on HOPG surface showing droplet nucleation and growth as humidity increases with time. Contrast artefacts in the second image are due to fluctuations in water vapour pressure during image acquisition. Obtained as pressure is raised from 700 Pa to 1300 Pa, and down to 500 Pa again, i.e. fully dehydrated. All images at same magnification. Pressure indicator show chamber pressure (white to blue) with respect to 100 % relative humidity (orange bar).

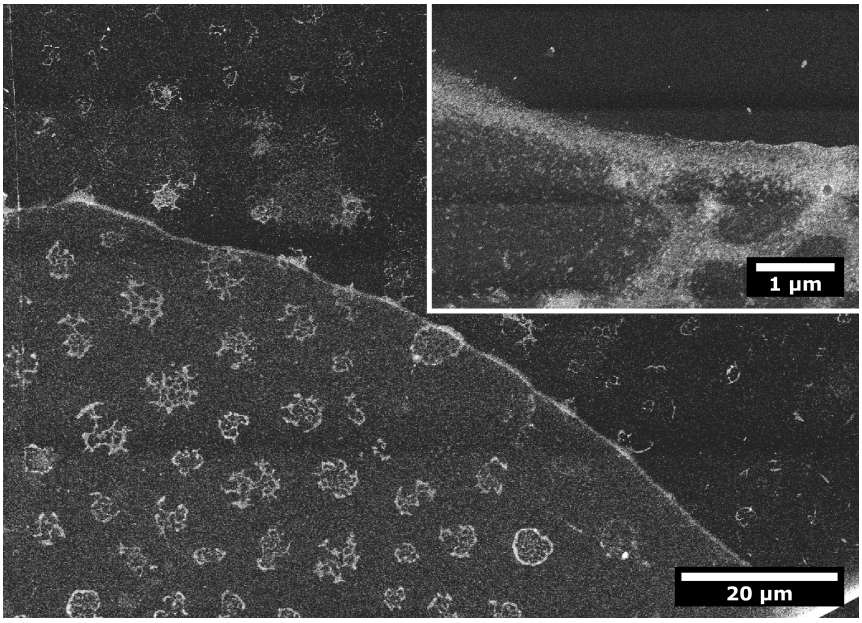

Fig. 4 GNPs on HOPG surface after wetting. Following the contour of a condensed water droplet, a new ring of GNPs is formed. The lighter background colour reflects the presence of redispersed particles (see inset). These individual particles become mobile during wetting and are rearranged on the surface upon drying.

will be discussed in more detail in section 3.6.

3.3 Wetting on Si

While nucleation of water droplets occurs on the deposits on hydrophilic GNP, similar to what has been observed on HOPG, the Si surface exhibited far better wetting properties resulting in localized water thin film formation (compare figure 5 *a* and *b*). In figure 5*c*+*d* this water thin film is clearly visible as it obscures the GNP structures. As the water content increases, more and more features are obscured by the growing water thin film. Note how the wetting front (dashed yellow line) to some extent follows the contours of the GNP structures (figure 5*d*).
Once the sample was dried again, it was clear that very small fraction of GNPs were actually dissolved and redeposited elsewhere (compare figure 5*e* with figure 5*f*, obtained before and after covering the features with water). It is clear that the local structure is maintained and only rafts of tightly bound particles have actually moved. Cracks also appear in the larger sheets, again indicating that these are tightly bound and move as one unit during hydration. We attribute this immobility to even stronger substrate-particle interactions than those observed on HOPG.

3.4 Wetting on PDMS

Wetting on a flat PDMS surface was also investigated. Figure ESI3† shows how a droplet of solution slowly dries out and forms the familiar ring pattern. The bulk of the sample surface was covered with tightly packed GNPs (see figure 2*c*). These form as the remaining water thin-film breaks down into smaller droplets and the high surface-tension forces the particles together. During hydration and the subsequent drying, all structural features, apart from the ring pattern, were completely rearranged. This is attributed to high surface mobility caused by the hydrophobic nature of the surface and its weak interaction with the PEG-coated GNPs.

3.5 Wetting on wrinkled PDMS

Similar to flat PDMS, when a droplet of GNP solution was deposited on the wrinkled PDMS surface and slowly dehydrated, ring formation occurred (see figure 6*a*). The structure of the bulk of the droplet (figure 6*b*)S contains GNPs covering the whole surface, but are predominantly deposited in the grooves of the substrate. These contain a few layers of particles, indicated by the brighter features in the image. As the surface consists predominantly of SiO_2 due to the plasma treatment, it is expected that the particles behave in a similar fashion to the Si surface (section 3.3) and cover entire substrate. Likewise, very low particle mobility was observed during and after evaporation of water of the sample suggesting a rather strong substrate-particle interaction.

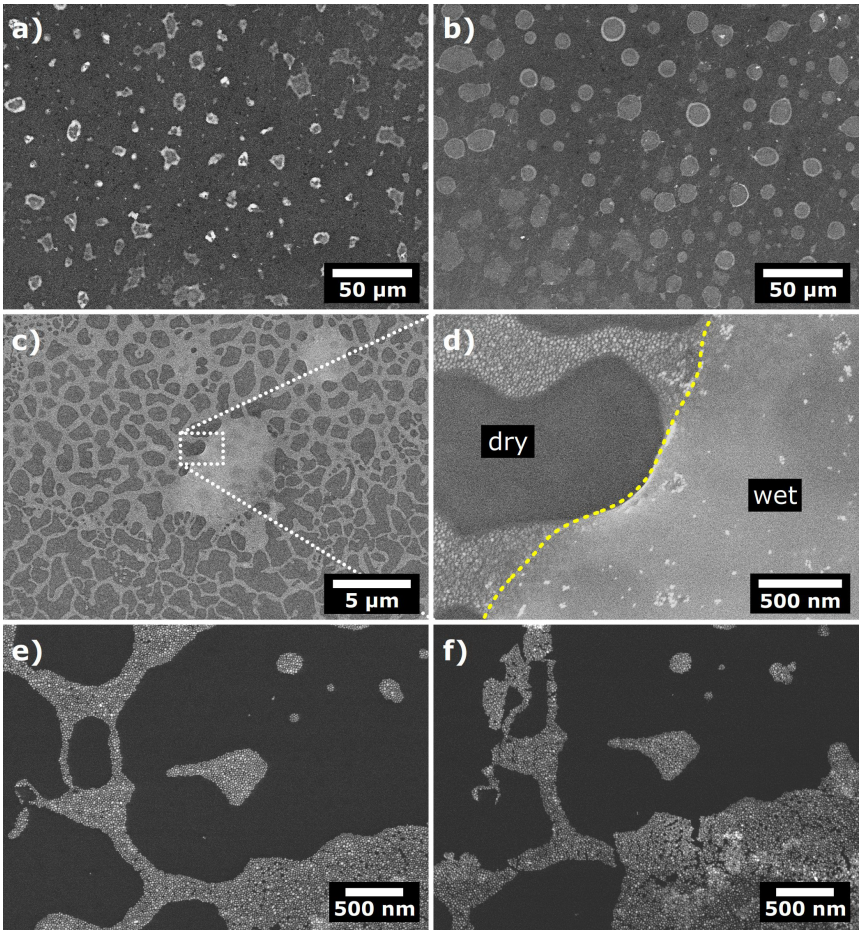

Fig. 5 Dry (*a*) and hydrated (*b-d*) Si surface, showing nucleation of water droplets on dense GNP aggregates. The condensed water droplets (shown in *c*) are clearly visible, marked by the wet/dry boundary (dotted yellow line in *d*). GNP structures rearrange only slightly during the wetting process as shown by comparing patterns before hydration (*e*) and after hydration and renewed drying (*f*).

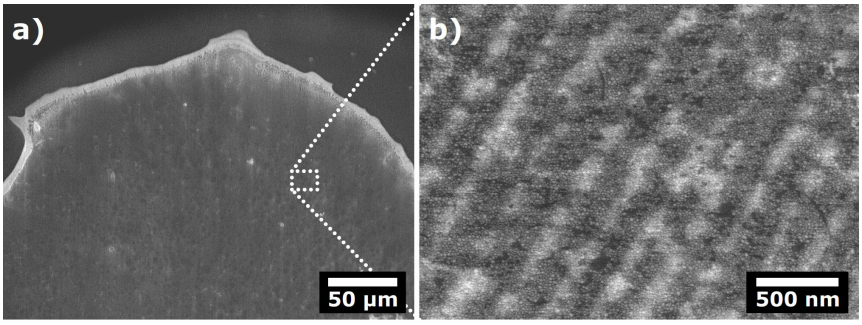

Fig. 6 GNPs deposited on wrinkled PDMS surface showing ring formation (*a*) and inner surface coverage (*b*) of grooves with GNPs.

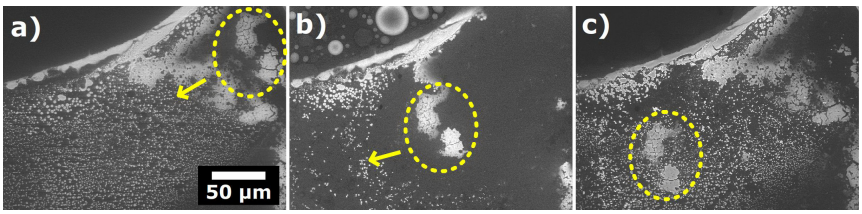

Fig. 7 Selected SEM images showing showing movement of large dense GNP sheets (yellow circle), before (*a*), during (*b*) and after (*c*) full surface hydration. All images at same magnification.

3.6 Particle mobility on wetted surfaces

In the previous sections it was observed that a large fraction of the GNP that were deposited on the surface during drying and wetting form ring patterns. In these rings the particles form very dense and strongly bound sheets, many monolayers thick. On all surface types, high mobility of these sheets was observed when water was present on the surface. Figure 7 shows GNPs on a HOPG surface, before, during and after hydration. Note the sheets (yellow circle) which have moved several hundred μm. It appears that the large coherent sheets of particles lift off the substrate and float on top of the water thin film. This was confirmed with high-magnification videos obtained in the ESEM during evaporation (see ESI4†) and condensation (see ESI5†) of small water droplets on a Si surface. In the videos we also show that particles which are still in contact with the substrate form continuous rafts together with those particles which already float on the water droplet. These findings correlate with those reported by Bigioni *et al.*, who reported self-assembly of nanocrystals floating on a water droplet (observed by optical microscopy).[51]

In addition, we observed that a portion of particles redispersed upon wetting and, when dried again, tended to deposit along structural features of the substrate step edges of HOPG and in the grooves of the wrinkled PDMS. Figure 8 shows GNPs concentrating around the lower part of graphite step-edges on the HOPG substrate. This is expected behaviour and can be attributed to entropically driven deposition.[52]

3.7 Role of soluble contaminants

In order to enhance entropically driven phenomena, highly soluble additives were added to the GNP dispersions. The rationale behind this approach is that solute molecules and GNPs in drying dispersions compete for available solvent volume. This can lead to the spontaneous crystallization of particles due a transient increase in entropy that stems from the release of the particles' covolume upon crystallization.[52]

We initially attempted to use glucose as an additive, but there were no noticeable effects on the types of GNP patterns formed, except for the presence of patches of poor electron density material which we attributed to the glucose. On the contrary, the addition of a highly water soluble salt (*nickel(II)-perchlorate*) had significant effects on the pattern formation.

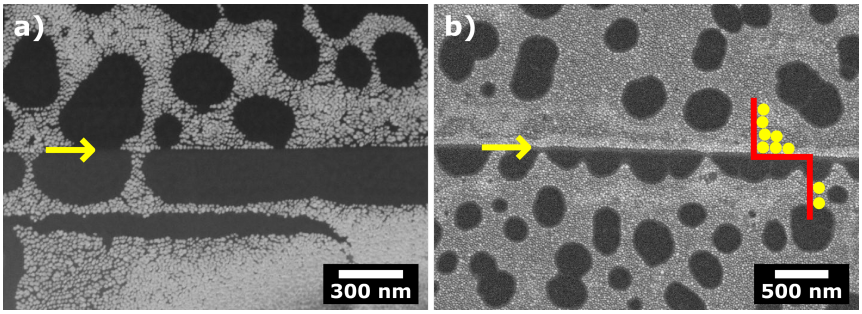

Fig. 8 SEM images showing GNP decoration of terrace edges (indicated by the arrow) on HOPG surfaces without (*a*) and with (*b*) nickel perchlorate. Sketch illustrating GNP packing in the z-direction is also presented in (*b*).

The wetting experiments in section 3.2, 3.3, 3.5 were now repeated with the nickel perchlorate solutions of GNPs (initial concentration 10 mM). Figure 9 shows image comparisons of drying patterns for HOPG and Si surfaces. The images clearly show a change in drying patterns on both hydrophobic (HOPG) and hydrophilic (Si) surfaces. On both substrates, particle packing appeared denser and consisted of a monolayer containing small holes, rather than the network of wormlike aggregates typical of spinodal phase separation observed in the absence of salt. We attribute this newly formed pattern to pinned hole nucleation, described previously in detail by Moriarty *et al.*.[20]
In the absence of the salt, some particles precipitate out early on the flat surfaces forming the structures observed (see figure 2), while others remain in solution and only precipitate out once the thin film of water has split into smaller droplets. This is what forms the large 3D clusters of particles. When salt is present, we get a salting out effect where all particles precipitate out earlier than in the case of the spinodal process. This happens while the water thin film is still almost continuous and hence monolayer formation and hole pinning are observed. This effect is termed entropic wetting[52] (of the particles on the substrate) and the preferential precipitation of the larger species (the GNP in this case) before the smaller (salt) is attributed to entropy gain as solvent volume is released when the particles precipitate on the surface. While the overall size of the droplet footprint did not change with addition of the salt, the number of particles present in 3D structures was greatly reduced, accounting for the denser packing overall surface coverage. Furthermore, on all samples containing nickel perchlorate we see formation of salt crystals on the surface (see images in ESI6†) when the sample was sufficiently dehydrated (below 20% humidity). This happens after the deposition of the GNP pattern.

When conducting the wetting experiments (condensing water), particle pattern formation in the presence of nickel perchlorate behave similarly to those without the salt. This means for the hydrophilic silicon surface almost no rearranging is detected (images not shown). On HOPG however high mobility was observed (see figure 10). Here the wormlike structures formed near the step edges during drying are completely restructured and larger flat sheets are formed instead, re-

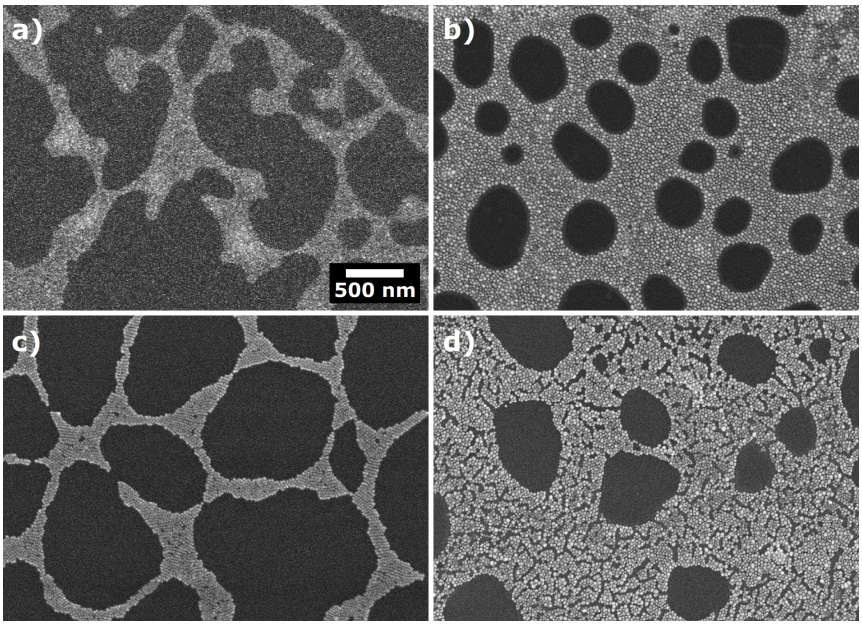

Fig. 9 Comparison of drying patterns of GNPs with no salt (*a*+*c*) and 10 mM nickel perchlorate (*b*+*d*) on HOPG (*a*+*b*) and Si (*c*+*d*). All images at same magnification.

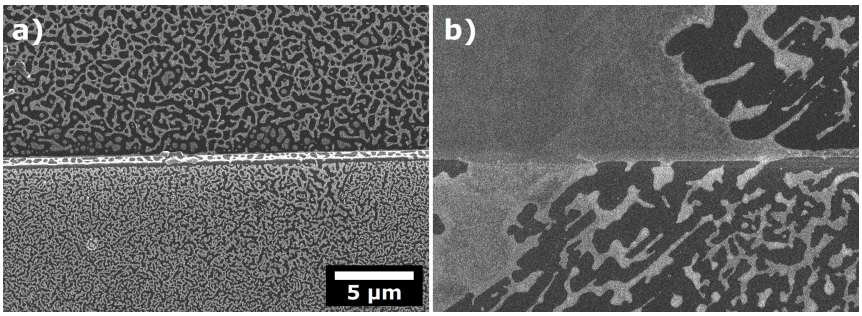

Fig. 10 Mobility of GNPs upon hydration on HOPG surface with 10 mM nickel perchlorate. Images obtained at the same spot before (*a*) and after (*b*) wetting. Both images at same magnification.

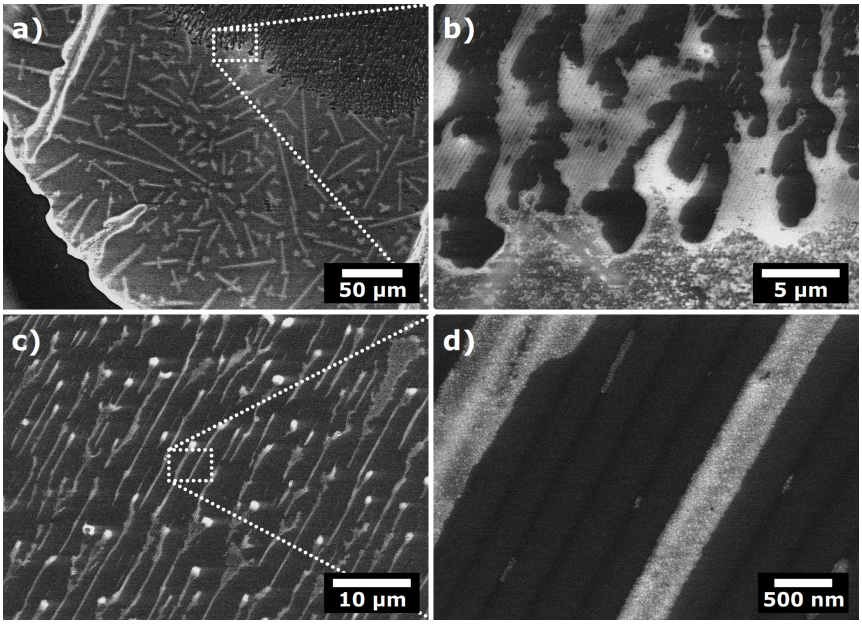

Fig. 11 SEM images showing GNPs precipitating on a wrinkled PDMS surface from a solution containing 10 mM nickel perchlorate. (a) Ring formation and salt-crystals formed at the droplet rim. (b) Viscous fingering at the interface between salt thin film and wrinkled PDMS surface. (c) "Tip" of the viscous fingers showing aggregates of particles. (d) GNPs deposited in the wrinkled PDMS groves as part of the "finger" structure.

sulting in a more homogeneous surface structure. Also, as noted earlier, there was a tendency to decorate the graphite step-edges.

On wrinkled PDMS, we observed a quite different behaviour (see figure 11). During drying the droplet separates into two distinct areas (see figure 11*a*). The outer structure contains a thin film of salt crystals (with GNPs dispersed inside it, figure 11*b*). The inner area contains only GNPs which have precipitated into the grooves of the wrinkled PDMS (figure 11*c*) and appear to have been formed by viscous fingering (figure 11*d*)[46]. This is indicative of the presence of a very thin water film that is gradually dewetting the substrate by evaporation. The particles accumulate at the dewetting front until the local concentration reaches a critical value at which they deposit as fingers. The structure of the surface clearly has an influence on the direction of the precipitation in these circumstances.

We have so far assumed that the nickel salt we used as a water soluble additive would not interact chemically with the particles or the substrate. Its only role was its need for solvent volume which is responsible for the entropically driven precipitation of GNPs. In order to test to what extend this assumption is valid, we have measured the zeta-potential of dispersions of particles at different concentrations of nickel perchlorate over a large range to reflect the scenario of an evaporating droplet (see figure 12). The Zeta-potential of our particles in the absence of nickel perchlorate is -44.8 mV $\pm$ 0.8 mV, potentially attributable to remaining adsorbed citrate molecules on the GNP surface. As soon as nickel per-

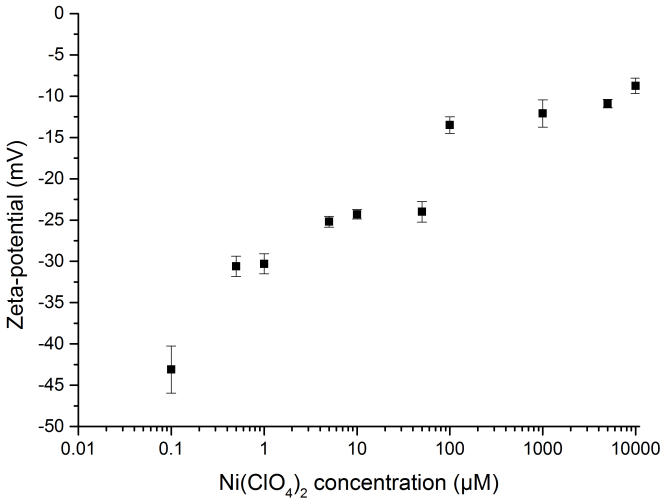

Fig. 12 Measured Zeta-potentials as function of nickel perchlorate concentration (note: log-scale on x-axis). Error bars indicate standard deviation.

chlorate is added, zeta-potential increases to less negative values, approximately extrapolating to zero at very high concentrations. This indicates a certain degree of complexation of Ni^{2+} by the PEG-ligand. This surprising result may account for the readiness by which more densely packed deposits are formed, since the nickel-loaded (and hence less charged) GNPs will experience less electrostatic repulsion from each other.

4 Conclusions

We have demonstrated by a series of typical nanoparticle deposition experiments that ESEM is a powerful tool to monitor nanoscale self-organization processes *in-situ* and in real time. While the choice of dispersant is limited to water, a range of very different substrates including insulators have been investigated, and a strong influence of substrate hydrophilicity and microstructure on the formation of the nanoscale patterns has been observed.

Surprisingly, once formed and attached to the substrate, a pattern of nanoparticles does not readily redisperse in condensed water droplets, but tends to either stick to the surface or lift off as a coherent raft of particles. This indicates that both substrate-particle and particle-particle interaction play an important role. Lift off of rafts and, to some extent, the formation of new rafts by particle aggregation on the droplet surface, can very nicely be seen at single particle resolution in the short movies provided as electronic supporting information.

All patterns observed could be rationalized by comparison with previously reported phenomena including spinodal phase separation, hole pinning, viscous fingering and entropic wetting. The latter was particularly evident in the presence of a nickel salt competing with the particles for accessible solvent volume. The findings summarized here represent our first ESEM study of nanoparticle

self-organisation and are still of preliminary nature. We expect that the opportunity to present this work at a Faraday Discussions meeting will yield significant additional insights which might guide future studies using this very promising technique.

Acknowledgements

Funding from the European Research Council (ERC) via the Advanced Grant PANDORA is gratefully acknowledged. We thank André Luis Fernandes Cauduro from the Mads Clausen Institute, University of Southern Denmark for preparing the structured PDMS surfaces.

References

1 P. Moriarty, *Rep. Prog. Phys.*, 2001, **3**, 297–381.
2 D. Vanmaekelbergh, *Nano Today*, 2011, **6**, 419–437.
3 A. Courty, A. Mermet, P. A. Albouy, E. Duval and M. P. Pileni, *Nat. Mater.*, 2005, **4**, 395–398.
4 M. Giersig and P. Mulvaney, *Langmuir*, 1993, **12**, 3408–3413.
5 M. Giersig and P. Mulvaney, *Annu. Rev. Phys. Chem.*, 1993, **24**, 6334–6336.
6 C. B. Murray, C. R. Kagan and M. G. Bawendi, *Science*, 1995, **270**, 1335–1338.
7 L. Motte, F. Billoudet and M. P. Pileni, *J. Phys. Chem.*, 1995, **44**, 16425–16429.
8 R. L. Whetten, J. T. Khoury, M. M. Alvarez, S. Murthy, I. Vezmar, Z. L. Wang, P. W. Stephens, C. L. Cleveland, W. D. Luedtke and U. Landman, *Adv. Mater.*, 1995, **8**, 428–433.
9 C. B. Murray, C. R. Kagan and M. G. Bawendi, *Annu. Rev. Mater. Sci.*, 2000, **30**, 545–610.
10 P. C. Ohara and W. M. Gelbart, *J. Phys. Chem.*, 1996, **32**, 13323–13329.
11 C. J. Kiely, J. Fink, M. Brust, D. Bethell and D. J. Schiffrin, *Nature*, 1998, 444–446.
12 C. J. Kiely, J. Fink, J. G. Zheng, M. Brust, D. Bethell and D. J. Schiffrin, *Adv. Mater.*, 2000, **12**, 640–643.
13 J. Fink, C. J. Kiely, D. Bethell and D. J. Schiffrin, *Chem. Mater.*, 1998, **3**, 922–926.
14 B. L. V. Prasad, C. M. Sorensen and K. J. Klabunde, *Chem. Soc. Rev.*, 2008, **37**, 1871–1883.
15 M. Brust and C. J. Kiely, *Colloids Surf., A*, 2002, **2-3**, 175–186.
16 P. C. Ohara and W. M. Gelbart, *Langmuir*, 1998, **12**, 3418–3424.
17 E. Rabani, D. R. Reichman, P. L. Geissler and L. E. Brus, *Nature*, 2003, **426**, 271–274.
18 G. Ge and L. Brus, *J. Phys. Chem. B*, 2000, **104**, 9573–9575.
19 M. Maillard, L. Motte, A. T. Ngo and M. P. Pileni, *J. Phys. Chem. B*, 2000, **104**, 11871–11877.
20 P. Moriarty, M. D. R. Taylor and M. Brust, *Phys. Rev. Lett.*, 2002, **89**, 248–303.
21 M. O. Blunt, C. P. Martin, M. Ahola-Tuomi, E. Pauliac-Vaujour, P. Sharp, P. Nativo, M. Brust and P. J. Moriarty, *Nat. Nanotechnol.*, 2007, **2**, 167–170.
22 J. Park, H. Zheng, W. C. Lee, P. L. Geissler, E. Rabani and P. A. Alivisatos, *ACS Nano*, 2012, **6**, 2078–2085.
23 L. Jiang, X. Chen, N. Lu and L. Chi, *Acc. Chem. Res.*, 2014, **47**, 3009–3017.
24 C. Hanske, M. Tebbe, C. Kuttner, V. Bieber, V. V. Tsukruk, M. Chanana, T. A. F. König and A. Fery, *Nano Lett.*, 2014, **14**, 6863–6871.
25 L. Jiang, Y. Sun, C. Nowak, A. Kibrom, C. Zou, J. Ma, H. Fuchs, S. Li, L. Chi and X. Chen, *ACS Nano*, 2011, **5**, 8288–8294.
26 T. Hassenkam, K. Norgaard, L. Iversen, C. Kiely, M. Brust and T. Bjornholm, *Adv. Mater.*, 2002, **14**, 1126–1130.
27 T. O. Hutchinson, Y. P. Liu, C. Kiely, C. J. Kiely and M. Brust, *Adv. Mater.*, 2001, **13**, 1800–1803.
28 J. Turkevich, P. C. Stevenson and J. Hillier, *Discuss. Faraday Soc.*, 1951, **11**, 55–75.
29 M. Morita, T. Ohmi, E. Hasegawa, M. Kawakami and K. Suma, *Appl. Phys. Lett.*, 1989, **55**, 562–564.
30 D. Janssen, R. Palma, S. Verlaak, P. Heremans and W. Dehaen, *Thin Solid Films*, 2006, **515**, 1433–1438.
31 F. Taherian, V. Marcon, N. F. A. van der Vegt and F. Leroy, *Langmuir*, 2013, **29**, 1457–1465.

32 S. Hu, X. Ren, M. Bachman, C. E. Sims, G. P. Li and N. Allbritton, *Anal. Chem.*, 2002, **74**, 4117–4123.
33 S. Hiltl, M. C. Shurings, A. Balaceanu, V. Mayorga, C. Leidel, A. Pich and A. Böker, *Soft Matter*, 2011, **7**, 8231–8238.
34 H. Alhummiany, S. Jarvis, R. A. J. Woolley, A. Stannard, M. Blunt and P. Moriarty, *J. Mater. Chem.*, 2011, **21**, 16983–16989.
35 I. Torchinsky, N. Amdursky, A. Inberg and G. Rosenman, *Appl. Phys. Lett.*, 2010, **96**, 093106.
36 M. Kolíbal, M. Konečný, F. Ligmajer, D. Škoda, T. Vystavěl, J. Zlámal, P. Varga and T. Šikola, *ACS Nano*, 2012, **6**, 10098–10106.
37 D. Aronov and M. Molotskii, *J. Appl. Phys.*, 2008, **104**, 114903.
38 D. Aronov, M. Molotskii and G. Rosenman, *Phys. Rev. B*, 2007, **76**, 035437.
39 D. Aronov, G. Rosenman and Z. Barkay, *J. Appl. Phys.*, 2007, **101**, 084901.
40 R. F. Egerton, P. Li and M. Malac, *Micron*, 2004, **35**, 399–409.
41 C. P. Royall, B. L. Thiel and A. M. Donald, *J. Microsc.*, 2001, **204**, 185–195.
42 K. Rykaczewski, J. Chinn, M. L. Walker, J. H. J. Scott, A. Chinn and W. Jones, *ACS Nano*, 2011, **5**, 9746–9754.
43 K. Rykaczewski and J. H. J. Scott, *ACS Nano*, 2011, **5**, 5962–5968.
44 L. Jiang, C. Zou, Z. Zhang, Y. Sun, Y. Jiang, W. Leow, B. Liedberg, S. Li and X. Chen, *Small*, 2014, **10**, 609–616.
45 Y. Noda, S.-I. Noro, T. Akutagawa and T. Nakamura, *Sci. Rep.*, 2014, **4**, 3758.
46 A. Stannard, *J. Phys. Condens. Matter*, 2011, **23**, 083001.
47 R. D. Deegan, O. Bakajin, T. F. Dupont, G. Huber, S. R. Nagel and T. A. Witten, *Phys. Rev. E*, 2000, **62**, 756–765.
48 W. Han and Z. Lin, *Angew. Chem. Int. Ed.*, 2012, **51**, 1534–1546.
49 Z. Y. Li, J. Yuan, Y. Chen, R. E. Palmer and J. P. Wilcoxon, *Adv. Mater.*, 2005, **17**, 2885–2888.
50 A. Dubavik, V. Lesnyak, N. Gaponik and A. Eychmüller, *Langmuir*, 2011, **16**, 10224–10227.
51 T. P. Bigioni, X.-M. Lin, T. T. Nguyen, E. I. Corwin, T. A. Witten and H. M. Jaeger, *Nat. Mater.*, 2006, **5**, 265–270.
52 A. D. Dinsmore, J. C. Crocker and A. G. Yodh, *Curr. Opin. Colloid Interface Sci.*, 1998, **1**, 5–11.

